JOURNAL OF BACTERIOLOGY, June 2006, p. 4542–4552 Vol. 188, No. 12
0021-9193/06/$08.00+0 doi:10.1128/JB.00122-06

Crystal Structure of Pyridoxal Kinase from the *Escherichia coli pdxK* Gene: Implications for the Classification of Pyridoxal Kinases

Martin K. Safo,[1]* Faik N. Musayev,[1] Martino L. di Salvo,[2] Sharyn Hunt,[1] Jean-Baptiste Claude,[3] and Verne Schirch[1]

Department of Medicinal Chemistry and Institute for Structural Biology and Drug Discovery, Virginia Commonwealth University, Richmond, Virginia 23219[1]; Dipartimento di Scienze Biochimiche A. Rossi Fanelli, Università La Sapienza, 00185 Roma, Italy[2]; and Information Génomique and Structurale (UPR CNRS 2589), 163 Avenue de Luminy, Case 934, 13288 Marseille Cedex 9, France[3]

Received 23 January 2006/Accepted 22 March 2006

The *pdxK* and *pdxY* genes have been found to code for pyridoxal kinases, enzymes involved in the pyridoxal phosphate salvage pathway. Two pyridoxal kinase structures have recently been published, including *Escherichia coli* pyridoxal kinase 2 (ePL kinase 2) and sheep pyridoxal kinase, products of the *pdxY* and *pdxK* genes, respectively. We now report the crystal structure of *E. coli* pyridoxal kinase 1 (ePL kinase 1), encoded by a *pdxK* gene, and an isoform of ePL kinase 2. The structures were determined in the unliganded and binary complexes with either MgATP or pyridoxal to 2.1-, 2.6-, and 3.2-Å resolutions, respectively. The active site of ePL kinase 1 does not show significant conformational change upon binding of either pyridoxal or MgATP. Like sheep PL kinase, ePL kinase 1 exhibits a sequential random mechanism. Unlike sheep pyridoxal kinase, ePL kinase 1 may not tolerate wide variation in the size and chemical nature of the 4′ substituent on the substrate. This is the result of differences in a key residue at position 59 on a loop (loop II) that partially forms the active site. Residue 59, which is His in ePL kinase 1, interacts with the formyl group at C-4′ of pyridoxal and may also determine if residues from another loop (loop I) can fill the active site in the absence of the substrate. Both loop I and loop II are suggested to play significant roles in the functions of PL kinases.

Pyridoxal 5′-phosphate (PLP) serves as a cofactor for many enzymes involved in amino acid and sugar metabolism. In many bacteria and plants, PLP is synthesized by a de novo pathway, but most cells rely on a nutritional source of vitamin B_6, i.e., pyridoxine (PN), pyridoxal (PL), and pyridoxamine (PM) (24). Most cell types have a salvage pathway for reutilizing the PL liberated during protein turnover (27). The salvage pathway involves an ATP-dependent pyridoxal kinase that phosphorylates PL, PN, and PM by transferring the terminal phosphate of ATP to the 5′-hydroxyl group of these substrates. The product of PN and PM phosphorylation is converted to PLP by pyridoxine 5′-phosphate oxidase, which is also expressed in most cells. The PL kinases that have been purified and studied show activity with PN and PM, in addition to PL, and are often referred to as PL/PN/PM kinases (14, 15). For brevity, we will refer to these enzymes as PL kinases with the understanding that many of them exhibit considerable activity with PN and PM.

PL kinase has been purified from bacterial, plant, and mammalian sources, and evidence suggests that most organisms contain a single PL kinase, coded by a *pdxK* gene. However, studies with *Escherichia coli* mutants that were blocked in the de novo biosynthetic pathway and with an inactivated *pdxK* gene, which codes for *E. coli* pyridoxal kinase 1 (ePL kinase 1), were still able to grow on pyridoxal (26). A search for a gene that expressed a protein that had PL kinase activity in *E. coli* led to the discovery of the *pdxY* gene (26). The *E. coli* protein ePL kinase 2, expressed by this gene, was shown to have some PL kinase activity, but at a greatly reduced level compared to the enzyme expressed by the *pdxK* gene (8, 26). It was postulated that the protein expressed by the *pdxY* gene was a kinase in another metabolic pathway, but with enough activity with PL as a substrate to support growth in the absence of the de novo biosynthetic pathway and ePL kinase 1. We have previously published the structure and kinetic properties of ePL kinase 2 (20). In addition, the crystal structure of sheep PL kinase, a product of a *pdxK* gene, has also been published (11, 12). PL kinase 2 and sheep PL kinase share 37% sequence identity, and as expected, the two proteins have similar structural folds. The sequence identity between ePL kinase 1, ePL kinase 2, and sheep PL kinase is ~30%. We now report the crystallographic and kinetic properties of *E. coli* PL kinase 1, expressed from the cloned *pdxK* gene. Comparison of the active-site/ATP binding site residues, active-site loops, functional properties, and sequence homologies suggest some unique features in the PL kinase family that can be used to classify these enzymes.

MATERIALS AND METHODS

Materials. All commercially available buffers and reagents were of the highest purity available. Pyridoxine 5′-phosphate (PNP) was prepared as previously described (25) and was further desalted by C_{18} reverse-phase high-performance liquid chromatography. 5′ Deoxy PL was prepared by the method of Cunningham and Thanassi (7). The *E. coli pdxK* gene (accession no. NC000913) was cloned into a pET22(+) vector and transformed into *E. coli* HMS 174(DE3) competent cells as described previously (8).

Expression and purification of ePL kinase 1. *E. coli* cells containing the cloned *pdxK* gene were grown in 6 liters of LB broth and, after reaching an optical density at 600 nm of 1.5, were induced with 0.2 mM IPTG (isopropyl-β-D-thiogalactopyranoside). The cells were grown for an additional 5 h at 30°C and

* Corresponding author. Mailing address: Department of Medicinal Chemistry and Institute for Structural Biology and Drug Discovery, 800 E. Leigh St., Virginia Commonwealth University, Richmond, VA 23219. Phone: (804) 828-7291. Fax: (804) 827-3664. E-mail: msafo@mail2.vcu.edu.

TABLE 1. Data collection and refinement statistics for *E. coli* PL kinase 1

Parameter	Value[a]		
	PL kinase 1	PL kinase 1 · ATP	PL kinase 1 · PL
Data collection statistics			
Unit cell parameters (Å)	65.31, 75.13, 107.80	65.13, 74.36, 107.21	63.67, 75.03, 109.36
Resolution limits (Å)	61.6-2.10 (2.20)	54.2-2.60 (2.70)	52.3-3.2 (3.3)
No. of measurements	143,009	61,122	25,322
No. of unique reflections	31,487	16,514	8,569
Redundancy	4.5 (4.1)	3.7 (3.2)	3.0 (2.9)
I/sigma *I*	9.8 (2.1)	9.9 (2.3)	9.3 (3.8)
Completeness (%)	99.3 (99.1)	99.2 (98.2)	94.2 (92.3)
R_{merge} (%)[b]	6.7 (24.8)	7.0 (22.2)	6.0 (10.6)
Structure refinement			
Resolution limit (Å)	19.87-2.10 (2.23)	19.94-2.6 (2.76)	19.90-3.2 (3.40)
Sigma cutoff (*F*)	0	1	1.5
No. of reflections	31,407 (4,837)	16,033 (2,402)	8,329 (1,194)
R factor (%)	19.4 (27.8)	20.7 (34.8)	23.4 (31.0)
R_{free} (%)	21.8 (27.8)	23.8 (37.2)	25.2 (34.5)
R_{msd} from standard geometry			
Bond length (Å)	0.006	0.009	0.009
Bond angle (degrees)	1.2	1.3	1.5
Average B values (Å^2)			
Protein/water atoms	34.5/42.3	47.42/38.89	33.74/26.4
Tris	39.5		
MgATP		68.65	
PL			54.61
Ramachandran plot (%)			
Most favored/additional	92.1/7.9	88.1/11.9	74/26
Coordinate errors (Luzzati plot)			
R factor	0.24	0.33	0.36
R_{free}	0.27	0.39	0.40

[a] Numbers in parentheses refer to the outermost resolution bin.
[b] $R_{merge} = \Sigma(<I> - I)/\Sigma I$.

harvested by centrifugation. The cell pellet was suspended in 200 ml of potassium phosphate buffer, pH 7.3, and ruptured by osmotic shock. After centrifugation, the expressed ePL kinase 1 was purified as previously described (8). The enzyme was greater than 95% pure as judged by sodium dodecyl sulfate-polyacrylamide gel electrophoresis.

Kinetic studies. Initial velocity studies for the conversion of PL to PLP were followed at 388 nm in an Agilant 8454 spectrophotometer in 50 mM potassium BES [*N*,*N*-bis(2-hydroxyethyl)-2-amino-ethanesulfonic acid], pH 7.3, at 37°C. PL concentrations were varied between 20 μM and 100 μM and ATP concentrations between 136 μM and 680 μM. The values for K_m and k_{cat} were determined from double-reciprocal plots constructed with Sigma Plot. Inhibition patterns and values of K_i were determined by double-reciprocal plots by varying the concentrations of the dead-end inhibitors 5-deoxy PL (120 to 320 μM), and AMP (0.2 to 0.6 mM).

Crystallization. The native (unliganded) ePL kinase 1 was screened using the hanging-drop vapor diffusion technique, and crystals grew in screens containing polyethylene glycol (PEG) 4K at 291 K. After optimization of the conditions, the best crystals were obtained from drops containing 3 μl of protein solution (21.5 mg/ml in 20 mM K phosphate, pH 7.5, 5 mM β-mercaptoethanol, 0.2 mM EDTA) and 3 μl of reservoir solution (21% PEG 4K, 100 mM Tris-HCl, pH 8.5, 200 mM Na acetate, 40 mM $MgSO_4$, and 10% glycerol).

Cocrystals of native protein with MgATP and PL were obtained by soaking unliganded crystals in mother liquid solutions containing 9 mM MgATP and 4.6 mM of pyridoxal. Attempts to directly cocrystallize the enzyme with PL and an ATP analog failed to give any crystals.

X-ray data collection and processing. For data collection, the unliganded crystal and MgATP-bound and PL-bound cocrystals were soaked for a few seconds in a solution containing 28% PEG 4K, 10% glycerol, 200 mM Na acetate, 40 mM $MgSO_4$, and 100 mM Tris-HCl buffer (pH 8.5) and quickly transferred to a liquid N_2 stream maintained at 100 K. The crystals diffracted to resolution limits of 2.1 Å, 2.6 Å, and 3.2 Å, respectively. Oscillation frames were measured using a rotating-anode X-ray generator operated at 50 mA and 100 kV and equipped with OSMIC confocal mirrors. An R-Axis II imaging-plate system was used as a detector. All crystals were orthorhombic and had a $P2_12_12_1$ space group. The Matthews coefficient of 2.16 and water content of 43% were consistent with one dimer per asymmetric unit. The data sets were processed with the BIOTEX program (Molecular Structure Corp.). Details of the data collection statistics are given in Table 1.

Structure of the unliganded ePL kinase 1. Attempts to solve the structure using the AMoRe molecular-replacement method (17) and multiple anomalous dispersion failed. Eventually, the crystal structure of the unliganded ePL kinase 1 was solved with the web tool CaspR, which executes an optimized molecular-replacement procedure using a combination of stand-alone software programs (6). The ePL kinase 1 sequence and three search models, ePL kinase 2 (Protein Data Bank [PDB] code 1TD2; 30% identity), sheep PL kinase (PDB code 1LHP; 30% identity), and 4-amino-5-hydroxymethyl-2-methylpyrimidine phosphate kinase from *Salmonella enterica* serovar Typhimurium (PDB code 1JXH; 27% identity), were first used to derive multiple structure-sequence alignments with the program T-Coffee (18), followed by homology model building with the program MODELLER (21). In all, 30 models were generated with different spatial conformations. Each model was automatically screened in a search for a molecular-replacement solution using AMoRe, followed by refinement using CNS (2). Two of the generated models had the best convergence, with a correlation coefficient and *R* factor of about 0.38 and 51%, respectively. The next-best solution had a correlation coefficient and *R* factor of 0.19 and 55%, respectively.

One of the molecular-replacement solution models with all nonglycine and nonalanine amino acids mutated to alanine was used for refinement. Residues from 118 to 122, 183, and 195 to 208 were deleted because of close contacts with

symmetry-related molecules. The refinement was performed with CNS, with a bulk solvent correction. The starting model was subjected to rigid body, positional, and simulated annealing using all 2.1-Å crystallographic data to an R factor/R_{free} of 46.8/52.1%. The refined model resulted in clear density for most of the amino acid side chains, which were then included in the model. More regions, comprising residues 1 to 9 and 130 to 138 and the C-terminal residues 281 to 283, were deleted because of weak density. Further cycles of refinement, with intermittent manual model corrections, resulted in an R factor/R_{free} of 40.3/45.8%, respectively, with more side chains added to the model. Due to the high R factors, as well as large errors in the model, the partially refined structure was used as a search model in AMoRE molecular replacement (with data to 3.0 Å), resulting in a correlation coefficient and R factor of 0.61 and 38%, respectively. Refinement of this model with CNS (with all data to 2.1 Å) resulted in a significant drop in the R factors/R_{free} (37/39.5%), as well as major improvement in the electron density map. Some of the deleted regions and the rest of the side chains were gradually built into the model during several cycles of refinement (each cycle consisted of positional and/or annealing and/or composite omit map and/or individual B-factor refinement with intermittent manual model correction). A total of 407 water molecules were also added to the model during the refinements. Two well-defined electron densities that matched Tris (used in the crystallization and cryoprotectant media) were also built into the model. The final model was refined to an R factor/R_{free} of 19.4/21.8% at 2.1 Å. Refinement statistics are summarized in Table 1. The graphics program TOM (3) was used for the manual model building.

Structure determination of the ATP- and PL-bound ePL kinase complexes. The refined unliganded ePL kinase 1 structure without the water and Tris molecules was used as the starting model to refine the MgATP-bound and PL-bound complex structures, respectively. A round of rigid body, positional, and simulated annealing refinements clearly showed ATP and PL bound at the active sites of the respective complexes, which were modeled in the structures. An Mg(II) ion and 163 water molecules were also included in the MgATP-bound complex, and the model was refined to a final R factor/R_{free} of 20.7/23.8% at 2.6 Å.

Due to the limited resolution of the PL-bound crystal, this complex was refined using noncrystallographic symmetry constraint (final weight, 2), mostly applied to sections of the structures that had a root mean square deviation (rmsd) of less than 0.8 Å between the two monomers (about 70% of the total structure). The model with 49 water molecules refined to a final R factor/R_{free} of 23.4/25.2% at 3.2 Å.

Protein structure accession numbers. The structural coordinates and structure factors for the unliganded, PL-bound, and MgATP-bound ePL kinases have been deposited in the Protein Data Bank with PDB codes 2DDM, 2DDO, and 2DDW, respectively.

RESULTS

Kinetic studies. ePL kinase 1 requires potassium as a monovalent cation. In the absence of any potassium ion, the activity is less than 5% of the maximum activity, and we cannot rule out the possibility that this residual low activity may be the result of some potassium ion in some of the reagents used in the assay. The half-maximal rate for potassium activation is 1.5 mM (data not shown). The presence of 100 mM NaCl does not alter the potassium activation profile.

The mechanism and kinetic constants for ePL kinase 1 were determined from double-reciprocal plots of initial rates with PL and MgATP as the variable and fixed substrates. In general, each substrate was varied over a 10-fold concentration range, which bracketed the respective K_m value. The pattern of lines in the double-reciprocal plots crossed on the negative x axis when either PL or ATP was the variable substrate, showing that there is no synergism in binding between these two substrates. The K_m values for PL and MgATP are shown in Table 2. The value of k_{cat} under assay conditions was 250 min^{-1}.

AMP and 5′-deoxy PL were used as dead-end inhibitors to aid in determining the mechanism of ePL kinase 1. Table 2 records the patterns observed and the constants derived from the double-reciprocal plots. The observation that dead-end inhibitors of both substrates gave only competitive and noncompetitive inhibition patterns suggests that the mechanism is sequential random addition of PL and ATP. However, a caution for this interpretation is the pattern observed when either PLP or PNP was used as a product inhibitor against MgATP. In each case, severe substrate inhibition by MgATP was observed. This inhibition is not explainable by the above-mentioned mechanism, suggesting that some possible control mechanism is operating for products of the kinase reaction (data not shown).

TABLE 2. Kinetic constants and inhibition patterns for *E. coli* PL kinase 1

Variable substrate	Inhibitor	K_m (μM)	K_i (mM)	Inhibition pattern
PL		50		
ATP		450		
PL	5′-Deoxy PL		0.20	Competitive
ATP	5′-Deoxy PL			Noncompetitive
PL	AMP			Noncompetitive
ATP	AMP		1.3	Competitive

Quality of the crystallographic models. The crystal structures of ePL kinase 1, its complex with MgATP, and the substrate PL are reported at resolutions of 2.1 Å, 2.6 Å, and 3.2 Å, respectively. All of the crystals belong to the orthorhombic space group, and the asymmetric unit of each structure contains monomers A and B, related by a noncrystallographic axis. The unliganded structure was the first to be determined using the web tool molecular-replacement method CaspR and was refined to a final crystallographic R factor/R_{free} of 19.4/21.8%. The model is missing residues 1 to 9, 197 to 203, and 281 to 283 from monomer A and 1, 132 to 137, 200 to 201, and 281 to 283 from monomer B. Also, residues 220 to 226 from both monomers show weak density. In addition, the model contains two Tris molecules at the active site. The unliganded structure was used as a starting model to refine the MgATP- and PL-bound complexes to R factor/R_{free} values of 20.7/23.8 and 23.4/25.2, respectively. Like the unliganded structure, the two ligand-bound complexes also have similar missing and weak regions. The MgATP-bound enzyme contains one ATP and one Mg(II) molecule at the active site of monomer A and the γ-phosphate of a disordered ATP at the active site of monomer B. The PL-bound enzyme also contains two PL molecules at both active sites of the protein. Refinement and other crystallographic parameters are listed in Table 1.

Overall structures. This is the first structure determination of a PL kinase from a prokaryote cell encoded by a *pdxK* gene; however, it is the third reported structure from the PL kinase family, which also includes ePL kinase 2, expressed by the *E. coli pdxY* gene (an isoform gene of p*dxK*), and sheep PL kinase, expressed by a eukaryote *pdxK* gene. These three PL kinase structures show the same typical ribokinase superfamily central core structure of β-strands surrounded by α-helices (4, 5, 11–13, 20, 22, 23, 28). Each monomer of ePL kinase 1 consists of eight α-helices and nine β-strands and is illustrated in Fig. 1A. The structure of the functional dimer is also shown in Fig. 1B. The buried surface area calculated with the CNS program suite is 3,120 $Å^2$ for the dimer. The corresponding values for the structural homologues, ePL kinase 2 and sheep PL kinase, are

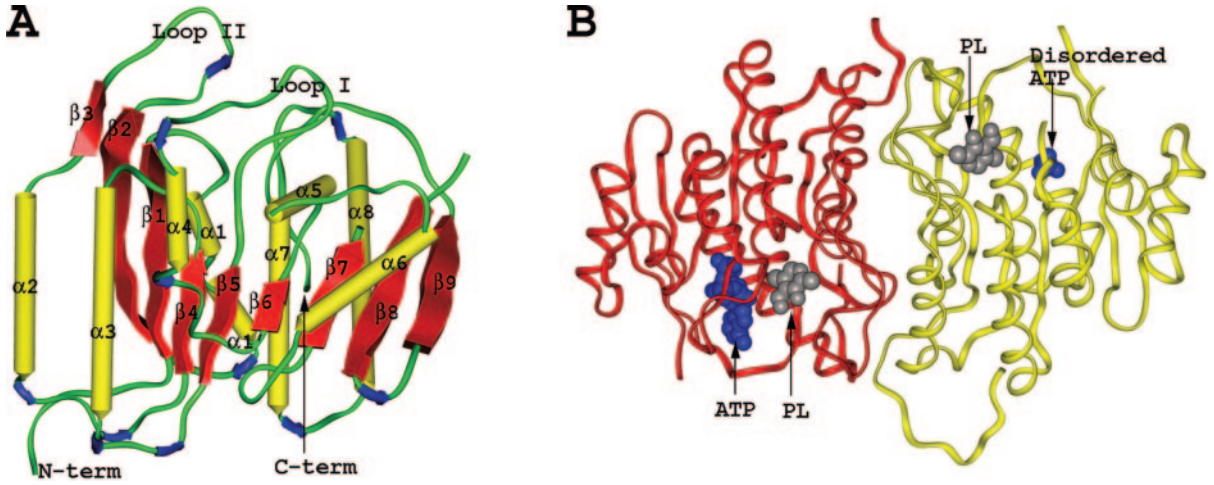

FIG. 1. Ribbon diagram of ePL kinase 1. (A) The monomeric structure of ePL kinase 1, with α-helices and β-strands colored yellow and red, respectively. The secondary structures are labeled. term, terminus. (B) The dimeric structure of the MgATP-bound complex superimposed with PL from the PL-bound complex. Monomer A and monomer B are in red and yellow, respectively. ATP and PL are shown as blue and gray spheres, respectively. The figures were generated with INSIGHTII (Molecular Simulations, Inc., San Diego, CA) and labeled with SHOWCASE.

3,410 and 3,860 Å^2, respectively (12, 20). There are two symmetry-related active sites in the dimeric structure of ePL kinase 1, each exclusively formed by residues from one monomer. Each dimeric structure superimposes on the other with significantly low rmsd (~0.4 Å for about 500 Cα pair atoms). Likewise, there are no significant differences between monomers within each structure, with the exception of the loops and turns, in most part due to disorder. Most noteworthy is the loop region located between the α4 helix and β5 strand (residues 129 to 137; loop I), which forms part of the active site (Fig. 1A).

ATP binding site. The crystal structure of the ATP-bound enzyme shows that the location of ATP and mode of interaction are very similar to those found in other ribokinases. Most notable are the hydrogen bond interactions between the ATP α-phosphate group and Thr231 and Gly232. Both residues are part of the anion hole motif (GTGD), comprised of residues Gly230, Thr231, Gly232, and Asp233. These residues, with the exception of Thr231, are the most conserved in the ribokinase superfamily and are known to bind phosphate and sulfate anions, as well as the ATP phosphates. The anion hole helps to neutralize negative charges and to stabilize the transition state during phosphate group transfer from ATP to the substrate, and in addition, Asp233 is believed to deprotonate the 5′ hydroxyl group of the substrate during catalysis (13, 22, 23). Other interactions involving the adenine ring, the sugar moiety, and the β- and γ-phosphates are depicted in Fig. 2A. Figure 2B and C shows the difference Fourier electron density (Fo-Fc) map (using phases before ATP was built into the model) and the Fourier (2Fo-Fc) map of the ATP, respectively. For the residues that make contact with the ATP, only Glu162, Gly232, Val224, and Met264 are either identical or conserved in the ribokinase superfamily structures.

Even though the crystal was soaked with MgATP for 3 days, we could identify only one complete ATP molecule, located at the active site of monomer A. In contrast, only the γ-phosphate and part of the β-phosphate of the ATP were observed at the active site of monomer B, suggesting that the whole ATP molecule binds at monomer B, but probably weakly and disordered beyond the γ-phosphate. This is consistent with a weak adenine ring density of the bound ATP at monomer A. Superimposition of the monomers among the three ePL kinase 1 structures shows that the ATP binding sites are structurally conserved with one exception. The side chains of Met206 and Arg223 in ePL kinase 1 are close to or occupy the adenine ring and ribose positions, respectively, in the monomers without bound ATP.

Comparison of the ATP binding site of ePL kinase 1 with that of either the binary ATP or the ternary ATP analog/PM complexes of sheep PL kinase shows that the largest deviation between the ATP positions occurs at the phosphate groups, especially at the γ-phosphate (Fig. 2F). In sheep PL kinase, the γ-phosphate is oriented closer to the mouth of the active site, while the corresponding γ-phosphate of ePL kinase 1 is oriented deeper into the inner core of the protein. In fact, the distance between the two γ-phosphorus atoms is about 4.7 Å. As a result of the different orientations of the ATP phosphate groups, the modes of interaction of the β- and γ-phosphate differ in the two structures. In ePL kinase 1, the γ-phosphate interacts with Asp125 and Glu162 (Fig. 2F), while the sheep enzyme γ-phosphate interacts with Tyr136 and Thr231. In addition, while the β-phosphate of ePL kinase makes a hydrogen bond interaction with Thr195, that of sheep makes contact with Asp130. We note that all the above-mentioned residues that make contact with the ATP phosphates in either enzyme are strictly conserved. The interaction of Asp130 and Tyr136 with the ATP phosphate groups in sheep PL kinase prompted Li and coworkers (11, 12) to suggest that these residues are essential in preventing premature hydrolysis of the γ-phosphate in PL kinases. This view was supported by the fact that a different orientation of loop I in monomer A of the binary ATP sheep complex abolished the contacts between the phosphate and the two residues Asp130 and Tyr136, resulting in a lack of electron density at the γ-phosphate position. Nevertheless, in ePL kinase 1, even though the γ-phosphate does not make hydrogen bond interactions with either the

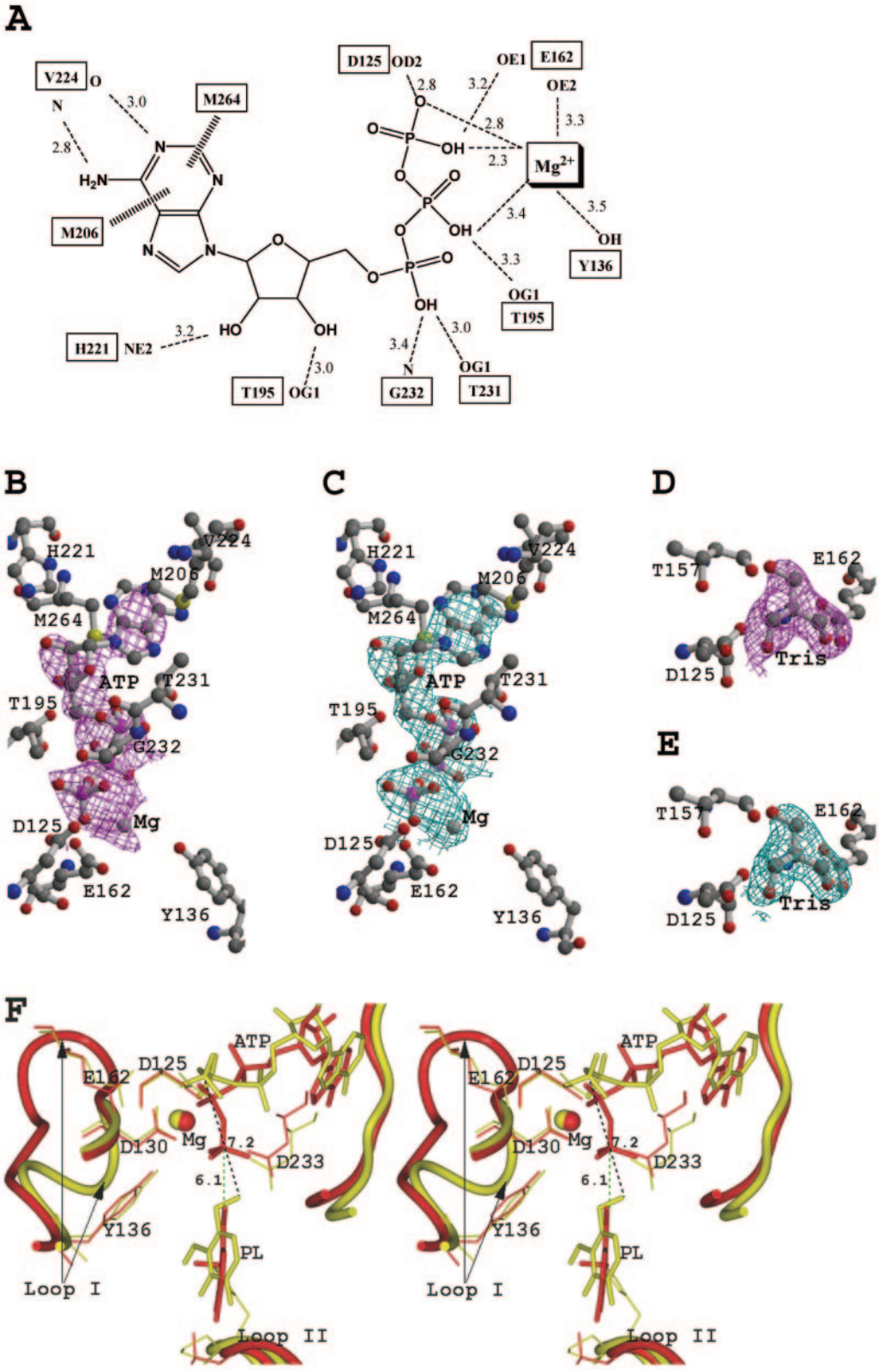

FIG. 2. The ATP binding site at monomer A. (A) Schematic diagram showing hydrophobic (broad dashed lines) and hydrogen bond (dashed lines) interactions between MgATP and the protein residues of the MgATP-bound complex. (B) An Fo-Fc map (contoured at 3.0 σ level) of magnesium and ATP of the MgATP-bound complex, calculated before magnesium and ATP were added to the model. (C) A 2Fo-Fc map (contoured at 1.0 σ level) of magnesium and ATP of the MgATP-bound complex. (D) An Fo-Fc map (contoured at 3.0 σ level) of Tris of the unliganded enzyme, calculated before Tris was added to the model. (E) A 2Fo-Fc map (contoured at 1.0 σ level) of Tris of the unliganded enzyme. All maps are superimposed on the final refined models. (F) Stereo view of superposition of the ATP and substrate binding sites of the binary ATP

conserved Asp130 or Tyr136, it is well resolved. Moreover, we note that if we were to rotate the ePL kinase 1 γ-phosphate group close to that of the sheep enzyme, Tyr136 of ePL kinase 1 could make hydrogen bond contact with the γ-phosphate group. However, there is no structural evidence to suggest such a γ-phosphate location occurs in ePL kinase 1. Clearly, the conclusion reached by Li and coworkers is not consistent with our observation in ePL kinase 1. Our structural analysis and the initial unbiased residual electron density map (Fig. 2B), as well as later omit maps in ePL kinase 1, clearly identify the ATP γ-phosphate, with its electron density contiguous with that of the β-phosphate. Also, the position of the ATP γ-phosphate in monomer A is consistent with the observed density of the γ- and part of the β-phosphates at the active site of monomer B. Moreover, in the unliganded ePL kinase 1 structure, we observed a Tris molecule that also occupied the same position as the ATP γ-phosphate (Fig. 2D and E). The Tris molecule makes hydrogen bond interactions with the residues Asp125 (2.5 Å), Glu162 (2.6 Å), and Thr157 (3.0 Å), as well as water-mediated hydrogen bond interactions with the protein. Interestingly, in the sheep PL kinase structure, there seems to be a contiguous electron density from the β-phosphate to the observed ePL kinase 1 γ-phosphate position, which the authors modeled with a potassium ion (see below).

We note that the sheep enzyme structure was determined with ZnATP, while we used MgATP, and the pH values of the experiments were different. ZnATP is a better substrate at pH 6, while MgATP is a better substrate at pH 7.3. This might explain the different γ-phosphate locations. We propose that Asp130 and Tyr136 may not be unique in protecting the γ-phosphate from premature hydrolysis, but any of the six residues Asp130, Tyr136, Asp125, Glu162, Thr195, and Thr231 could serve that function. One thing is certain: in both binary ATP enzyme structures, as well as the ternary ATP analog/PM sheep structure, the γ-phosphate is very distant from the putative substrate (>6 Å) (Fig. 2F), and the ATP and substrate would have to move toward each other to effect catalysis.

Metal binding sites. The crystallization medium contains the metal ions Mg^{2+}, K^+, and Na^+. Mg(II) ion was modeled into a residual density adjacent to the ATP γ-phosphate (Fig. 2B). The coordination of the Mg^{2+} ion appears to be square-pyrimidal. It makes hydrogen bond interactions with the β/γ-phosphate (2.3 Å, 2.8 Å, and 3.4 Å), as well as with the residues Tyr136 (3.5 Å) and Glu162 (3.2 Å). However, a weak residual density, most likely a water molecule (not included in the model; ~3.5 Å from the Mg^{2+} ion) could bind to the metal ion, resulting in an octahedral coordination geometry around the magnesium. Magnesium is needed by the kinases for catalysis, but the sheep enzyme was reported to exhibit higher activity in the presence of Zn(II) at pH 6 (12). The Mg(II) ion overlaps the Zn(II) ion position found in the sheep PL kinase structure (12). The position of the potassium ion in the ePL kinase 1 enzyme is less certain, and as a result, we did not model any monovalent ion in the ePL kinase 1 structure. It is interesting that the putative K^+ ion in sheep PL kinase is located where the γ-phosphate in ePL kinase 1 is observed. The K^+ ion positions are different for many of the ribokinases (28). Binding of K^+ ion to the anion hole or to the ATP phosphate is believed to activate the kinase enzyme (1, 10, 12, 14, 15, 28).

Pyridoxal binding site. Figure 3A and B depicts the interactions between PL and the active-site residues in ePL kinase 1, while Fig. 3C and D shows the difference Fourier electron density map (using phases before PL was built into the model) and the 2Fo-Fc map of PL, respectively. The bound PL superimposes closely on the bound substrates in sheep PL kinase and ePL kinase 2 (Fig. 3E). Likewise, the geometry of the substrate binding site and the overall position of the substrate are similar to those of the other ribokinase superfamily members, especially those of 4-amino-5-hydroxymethyl-2-methylpyrimidine phosphate kinase (5). There are several distinct structural features of the active site that contribute to the binding of the substrate and/or shield the substrate during catalysis. These include two loop structures that guard the active site. First, the flexible loop I (residues 129 to 137), which is commonly referred to as a flap or lid in the ribokinase superfamily, was found to be in a partially opened position in monomer A. The corresponding loop I in monomer B, residues 132 to 137, is missing. It appears that extensive crystal contact interactions led to stabilization of the loop at monomer A, but we cannot rule out asymmetry in the dimer solution, which has also been suggested for other ribokinase superfamily members (28). The loops are similar in the three PL kinase structures and the non-PL ribokinase 4-amino-5-hydroxymethyl-2-methylpyrimidine phosphate kinase structure; however, the loop in sheep PL kinase is three residues longer. Interestingly, the loop packs closely and makes direct contact with the substrate in ePL kinase 2, while in ePL kinase 1, sheep PL kinase, and 4-amino-5-hydroxymethyl-2-methylpyrimidine phosphate kinase, there are no direct contacts between the loop residues and the corresponding substrates (Fig. 3E).

Second, loop II (located between strands β2 and β3, residues 55 to 64) shields and contributes a binding motif (Pro-His) of residues Pro58 and His59 that makes hydrophobic and hydrogen bond interactions with O-3′- and C-4′-oxygen of PL, respectively (Fig. 3). In addition to having interactions with the substrate, the side chain of His59 is also strategically located to provide cover to the active site from the solvent. The sequence Pro-His in the loop II binding motif is mostly conserved in the *pdxK* gene products, especially those with high sequence homology with ePL kinase 1. The sequence in the binding motif is replaced by Thr-Gln in the *pdxY* gene products. However, there is no systematic conservation of these residues in the non-PL ribokinases. Unlike loop I, the sizes and conformations of loop II are very similar in ePL kinase 1, sheep PL kinase, and ePL kinase 2, which remains in a closed conformation

complex of ePL kinase (colored yellow) and the ternary ATP analog/PM complex of sheep kinase (colored red). PL from the PL-bound ePL kinase 1 complex was superimposed on the MgATP-bound ePL kinase 1 complex. The protein is shown in ribbons. The ATP and PL and the binding site residues are shown as sticks, while the divalent ions are shown as spheres. For clarity, not all binding site residues are shown. Panel A was made using ChemDraw 9.0. Panels B to E were drawn using BOBSCRIPT (9) and RASTER3D (16) and labeled using SHOWCASE (Silicon Graphics, Inc.). Panel F was generated with INSIGHTII and labeled with SHOWCASE.

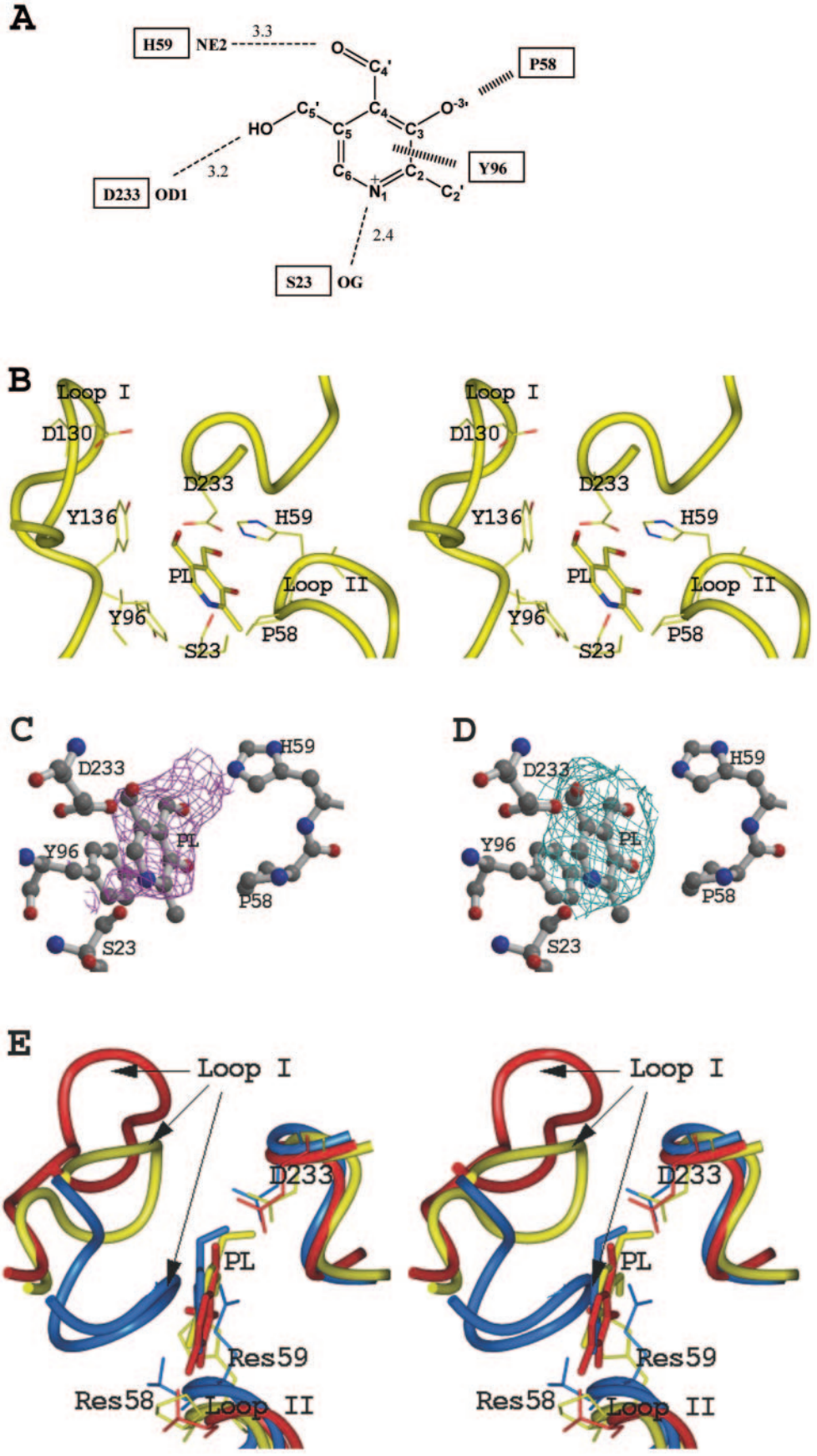
A
H59
NE2
3.3
P58
HO
3.2
D233
OD1
Y96
2.4
S23
OG
B
Loop I
D130
Y136
Y96
D233
H59
PL
Loop II
S23
P58
C
D233
H59
Y96
PL
S23
P58
D
D233
H59
Y96
PL
S23
P58
E
Loop I
D233
PL
Res59
Res58
Loop II

whether the enzyme is liganded or not. Its role is probably to sequester the substrate for catalysis (20), among other possible functions (see below). As will be discussed below, perhaps His59 may also serve to prevent loop I from moving into the substrate binding site of ePL kinase 1. In sheep PL kinase, His59 is replaced by Gly, and the loop is observed to move into the substrate site (12).

Other important PL-binding residues include Ser23 and Asp233, making hydrogen bonds with the N1 and C5′ hydroxyl atoms, respectively. Finally, there is a π-π stack interaction between the PL ring and Tyr96 that may help to orient the molecule for proper interaction and catalysis. These three residues are completely conserved in the PL kinases; however, only Asp233 is highly conserved in the ribokinase superfamily.

DISCUSSION

E. coli expresses PL kinases from the *pdxK* and *pdxY* genes (8). Previously, we reported on ePL kinase 2, encoded by the *pdxY* gene (20). This enzyme has very low activity and binds PL covalently at the active site. The true function of this protein in *E. coli* is unknown. The major activity for PL kinase is expressed by the *pdxK* gene, and it is this ePL kinase 1 that is described in this study. It appears that the mechanism is sequential random addition of substrates, which is in agreement with the mechanism found for the sheep PL kinase. This mechanism is consistent with the observation that binary complexes of ePL kinase 1 with PL and MgATP form in the crystal. Although other PL kinases have been described as using ZnATP, we have previously shown that these studies were done at low pH and far from physiological conditions. Not only is there not enough free Zn^{2+} in the cell to form significant amounts of ZnATP, but under physiological conditions, MgATP is a better substrate. ePL kinase 1 also requires potassium for activation.

If we superimpose either PL on the binary ATP-bound ePL kinase complex or ATP on the binary PL-bound complex (Fig. 2F), we find that the C-5′-hydroxyl group of PL is ~7 Å from the γ-phosphate of ATP, suggesting that the catalytic conformation may be significantly different from that of either complex observed in the crystal. A similar observation was reported for both the binary ATP and the ternary ATP analog/PM complexes of sheep PL kinase (11, 12), where the ATP γ-phosphate was observed to be about 6 Å from the 5′-hydroxyl group of the substrate (Fig. 2F). This prompted the authors to speculate that the ternary complex observed in the crystal structure must undergo a further conformational change to a transition state ("prereaction state") that places the phosphate and the substrate closer together to allow transfer of phosphate from ATP to the substrate (11). The structure of this catalytically active ternary complex awaits further study.

Structural comparison with the ribokinase superfamily. In addition to the three PL kinase structures, there are also eight closely related non-PL ribokinase superfamily structural homologues. A comprehensive analysis of the ribokinase superfamily of proteins has been reported previously (4, 5, 12, 13, 23, 28).

A characteristic feature in the ribokinase superfamily structures is a flap or lid that covers the substrate, as well as the ATP phosphate groups. This structural feature has been suggested to be significant in substrate binding and/or catalysis and has been used to propose an evolutionary pathway for the enzymes (4, 5, 12, 28). In the three PL kinase structures (ePL kinase 1, ePL kinase 2, and sheep PL kinase), the flap is defined by loop I (Fig. 1A, 2F, and 3E).

The flap is unique in sheep PL kinase compared with those of ePL kinase 1 and ePL kinase 2. In both monomers of the unliganded sheep PL kinase structure (PDB code 1LHP) and in monomer A of the ATP-bound sheep PL kinase structure (PDB code 1LHR), the flap completely occupies the putative substrate position (not shown in the figures). In contrast, in monomer B of the ATP-bound sheep enzyme, loop I has swung out of the active site and clearly opens it to solvent access. In this conformation, the residues Asp130 and Tyr136 located on loop I are able to interact with the β/γ-phosphates of ATP and, as suggested by Li et al., (11, 12), protect the γ-phosphate from premature hydrolysis. Even though the ePL kinase 1 mechanism is the same as that of the sheep PL kinase, none of the ePL kinase 1 structures (either unliganded or ATP bound) shows any movement of loop I into the substrate site. We noted that the loop is three residues shorter in ePL kinase 1 than in sheep PL kinase (Fig. 2F and 3E). The rotation of loop I into the substrate binding site in sheep PL kinase was suggested to be due to crystal packing, but it is not apparent if this event could occur in ePL kinase 1. Loop I may be too short in ePL kinase 1 to rotate and move into the substrate site, and in addition, its movement into the substrate site may be restricted by possible steric interaction with the loop II residue His59. In sheep PL kinase, residue 59 is glycine. Like ePL kinase 1, both ePL kinase 2 and 4-amino-5-hydroxymethyl-2-methylpyrimidine phosphate kinase, also with similar shorter loops, did not show loop I occupying the substrate binding sites.

Comparison of PL kinases. A FASTA (19) search using the ePL kinase 1 sequence revealed more than 100 close homologues of PL kinases from both prokaryotes and eukaryotes (Fig. 4). The species with sequence identities to ePL kinase 1 ranging from 28 to 99% are encoded by two main genes, *pdxY* and *pdxK*. At this point, we have not been able to find homo-

FIG. 3. The substrate binding site at monomer A of the PL-bound complex. (A) Schematic diagram showing the hydrophobic (broad dashed lines) and hydrogen-bond (dashed lines) interactions between PL and the active-site residues. (B) Stereo view of the PL binding site, with the protein shown in yellow ribbons. The PL and the residue side chains are shown as yellow sticks, with oxygen and nitrogen atoms colored red and blue, respectively. For clarity, not all of the active-site residues are shown. (C) An Fo-Fc map (contoured at 2.5 σ level) of PL, calculated before it was built into the model. (D) A 2Fo-Fc map of PL, contoured at 0.8 σ level. All maps are superimposed on the final refined model. (E) Stereo view of superposition of the substrate binding sites of ePL kinase 1 (colored yellow), ePL kinase 2 (colored blue), and sheep PL kinase (colored red). Panel A was made using ChemDraw 9.0. Panels B and E were generated with INSIGHTII and labeled with SHOWCASE. Panels C and D were drawn using BOBSCRIPT (9) and RASTER3D (16) and labeled using SHOWCASE (Silicon Graphics, Inc).

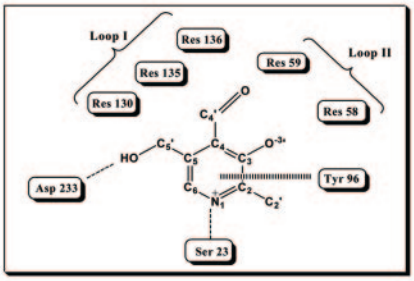

PL Kinase Source	ID (%)	23	58	59	96	130	135	136	233
A. Prokaryote (*pdxK* gene product)									
Escherichia coli (P40191)	---	S	P	H	Y	D	I	Y	D
Shigella flexneri (Q7UC31)	99	S	P	H	Y	D	I	Y	D
Salmonella typhimurium (P40192)	68	S	P	H	Y	D	M	Y	D
Salmonella paratyphi-a (Q5PNC8)	68	S	P	H	Y	D	M	Y	D
Bordetella pertussis (Q7VYK4)	48	S	P	H	Y	D	V	Y	D
Bordetella bronchiseptica (Q7WII1)	48	S	P	H	Y	D	V	Y	D
Rhodopseudomonas palustris (Q6N619)	31	S	P	G	Y	D	V	F	D
Agrobacterium tumefaciens (Q8UCJ7)	29	S	P	G	Y	D	L	Y	D
B. Eukaryote (*pdxK* gene product)									
Ovis aries; Sheep (P82197)	30	S	T	G	Y	D	M	Y	D
Sus scrofa; Pig (O46560)	28	S	T	G	Y	D	M	Y	D
Homo sapiens; Human (O00764)	28	S	T	G	Y	D	M	Y	D
Rattus norvegicus; Rat (O35331)	27	S	T	G	Y	D	M	Y	D
Arabidopsis thaliana; mouse (Q8W1X2)	30	S	T	G	Y	D	L	Y	D
C. Prokaryote (*pdxY* gene product)									
Escherichia coli (P77150)	30	S	T	Q	Y	H	C	I	D
Shigella flexneri (Q83KY1)	30	S	T	Q	Y	H	C	I	D
Salmonella typhimurium (Q8ZPM8)	30	S	T	Q	Y	H	C	I	D
Salmonella paratyphi-a (Q5PIK8)	29	S	T	Q	Y	H	C	I	D
Yersinia pestis (Q8ZE21)	31	S	T	Q	Y	H	C	I	D
Pasteurella multocida (Q9CNY1)	30	S	T	Q	Y	H	C	I	D
Pseudomonas putida (Q88C26)	27	S	T	Q	Y	H	C	I	D
Pseudomonas syringae (Q87TZ6)	31	S	T	Q	Y	H	C	I	D
Haemophilus influenzae (P44690)	28	S	T	Q	Y	H	C	I	D

FIG. 4. Active-site residues among selected members of PL kinases. The figure at the top roughly shows the active-site residues relative to the substrate moieties. The residues are numbered according to ePL kinase 1 notation. The proteins are divided into three groups based on the gene source and the cell type. (A) PL kinases expressed by *pdxK* genes of prokaryotes. (B) PL kinases expressed by *pdxK* genes of eukaryotes. (C) PL kinases expressed by *pdxY* genes of prokaryotes. The database identifier numbers are shown in parentheses. The sequence identity between ePL kinase 1 and the rest of the PL kinases are shown in column 2. Residues 23, 96, and 233 (colored black) are conserved in all the PL kinases. Residues 58 and 59 are located on loop II, and the sequence is almost always Thr-Gln (colored blue) in the *pdxY* gene products. There are three different binding motifs of residues 58 and 59 in the *pdxK* gene products: Pro-His (colored red) in the prokaryotes that have high sequence identity with ePL kinase 1 (40 to 99%), Pro-Gly (colored green) in the prokaryotes that have low sequence identity with ePL kinase 1 (~30%), and Thr-Gly (colored magenta) in the eukaryotes, also with low sequence identity with ePL kinase 1 (~30%). Residues 130, 135, and 136 are located on loop I. In the *pdxK* gene products, these residues are conserved and are mostly Asp-X-Tyr (colored red), where X is I, M, L, or V. These residues are replaced by His-Cys-Ile (colored blue) in the *pdxY* gene products. The sequence alignment figure was generated with ClustalW in the FASTA program (19), while the diagram was made using ChemDraw 9.0.

logues of *pdxY* in eukaryotes. Some prokaryotes have both gene types. Interestingly, the sequence identity between isoforms of the same species is very low (~30%) compared to the high sequence identity between different species for the same gene.

There are two unique features at the active site that separate the *pdxY* and *pdxK* gene products. First, the residues Asp130, Ile135, and Tyr136 located on loop I are conserved in the *pdxK* species but are replaced mainly by His, Cys, and Ile in the *pdxY* proteins (Fig. 4). As noted for the sheep PL kinase structure, Asp130 and Tyr136 are believed to interact with the ATP phosphates to prevent premature ATP hydrolysis. Both Asp130 and Tyr136 are conserved in ePL kinase 1, but neither interacts with the phosphate groups. In ePL kinase 2, where Ile is replaced by Cys135, this residue was observed to be covalently attached to PL as a possible thiohemiacetal adduct.

The second unique active-site feature is the two-residue loop II binding motif (residues 58 and 59) (Fig. 3E and 4). In the *pdxK* gene products, there are three distinct binding motifs, including Pro-His, Thr-Gly, and Pro-Gly, in contrast to the *pdxY* gene products, where residues 58 and 59 are almost always Thr-Gln (Fig. 4). In ePL kinase 2, Thr58 and Gln59 are involved in hydrogen bond interactions with O-3′- and C-4′-oxygen of the substrate, respectively (20). The corresponding motifs in ePL kinase 1 and sheep PL kinase are Pro-His and Thr-Gly, respectively, where Thr58 and His59 make hydrogen bond interactions with the O-3′- and C-4′-oxygen of the corresponding substrates, respectively. While residue 58 is buried, residue 59 is located close to the mouth of the active site, and as the side chain of the latter residue gets longer, it shields the active site from the bulk solvent, and in particular, the C-4′ position of the substrate. Residue 59 is Gly in sheep PL kinase, and the absence of a side chain leaves the C-4′ position of the substrate uncovered and allows easy access to the active site from the solvent and filling of the active site by loop I. We hypothesize that this two-residue binding motif on loop II may be an important fingerprint region in the PL kinase proteins by helping to sequester the substrate and perhaps determining substrate specificity, as well as kinetic activity.

In the *pdxK* gene products, those species with the highest sequence identity to ePL kinase 1 (40 to 99%) are all prokaryotes and have similar ePL kinase 1 binding motifs of either Pro-His or Pro-Arg (residues 58 and 59). Like ePL kinase 1, it is hypothesized that residue 59 would cover and make hydrogen bond interaction with the C-4′ substituent of the substrate, as well as prevent loop I from entering the substrate site. In the prokaryotic kinases, also expressed from the *pdxK* genes with a lower sequence identity of only ~30% to ePL kinase 1, the binding motif is Pro-Gly. These sequences would neither provide hydrogen bond capability to the substrate nor prevent loop I from entering the substrate site. Finally, in the rest of the *pdxK* proteins (all eukaryotic and with sequence identities of ~30% to ePL kinase 1), the binding motif is Thr-Gly. Like sheep PL kinase, Thr58 would most likely make hydrogen bond interaction with the O-3′ of the substrate, while the lack of a side chain at residue 59 may allow loop I to enter the substrate binding site.

Substrate specificity in PL kinases. McCormick and Snell (15) reported that pyridoxal kinases from rat, human, and yeast show tolerance to a wide variation of substitutions at the C-4′ position of pyridoxal. In contrast, the bacterial kinases from *Lactobacillus casei* and *Streptococcus faecalis* were found to have lower affinities for different substituents at the C-4′ position (15). The tolerance for the variation of the C-4′ substituents in eukaryotic systems could be explained by the nature of the loop II binding motif. In the crystallographic studies of ePL kinase 1, ePL kinase 2, and sheep PL kinase, it was observed that the C-4′ position of the substrate is adjacent to residue 59. In ePL kinase 1 and ePL kinase 2, this residue is His and Gln, respectively, which make hydrogen bond interaction with the formyl group at C-4′ and provide cover for the C-4′ position of the substrate from bulk solvent. In mammals and yeast kinases, residue 59 is glycine and would likely leave the C-4′ position of the substrate open to bulk solvent. This is confirmed by the crystal structure of sheep PL kinase, which shows the C-4′ position of the substrate uncovered, explaining the tolerances of these enzymes for different substituents at position C-4′ of PL or its derivatives. The sequences of *Lactobacillus casei* and *Streptococcus faecalis* are not available; however, it is most likely that residues 59 in the PL kinase enzymes from both prokaryotes do make hydrogen bond contact with the C-4′ position of the substrate.

ACKNOWLEDGMENTS

This work was supported by NIH grant DK56648 (V.S.) and by grant COFIN2003 from the Italian Ministero dell'Istruzione, dell'Università e della Ricerca (M.L.D.S.)

We thank Marcella Guiso from the Department of Chemistry of Università La Sapienza, Roma, Italy, for helping with the synthesis of 5′-deoxy PL.

REFERENCES

1. **Andersson, C. E., and S. L. Mowbray.** 2002. Activation of ribokinase by monovalent cations. J. Mol. Biol. **315:**409–419.
2. **Brunger, A. T., P. D. Adams, G. M. Clore, W. L. DeLano, P. Gros, R. W. Grosse-Kunstleve, J. S. Jiang, J. Kuszewski, M. Nilges, N. S. Pannu, R. J. Read, L. M. Rice, T. Simonson, and G. L. Warren.** 1998. Crystallography and NMR system: a new software suite for macromolecular structure determination. Acta Crystallogr. D **54:**905–921.
3. **Cambillau, C., and E. Horjales.** 1987. TOM: a Frodo subpackage for protein-ligand fitting with interactive energy minimization. J. Mol. Graph. **5:**174–177.
4. **Campobasso, N., I. I. Mathews, T. P. Begley, and S. E. Ealick.** 2000. Crystal structure of 4-methyl-5-beta-hydroxyethylthiazole kinase from *Bacillus subtilis* at 1.5 Å resolution. Biochemistry **39:**7868–7877.
5. **Cheng, G., E. M. Bennett, T. P. Begley, and S. E. Ealick.** 2002. Crystal structure of 4-amino-5-hydroymethyl-2-methylpyrimidine phosphate kinase from *Salmonella typhimurium* at 2.3 Å resolution. Structure **10:**225–235.
6. **Claude, J. B., K. Suhre, C. Notredame, J. M. Claverie, and C. Abergel.** 2004. CaspR: a web server for automated molecular replacement using homology modelling. Nucleic Acids Res. **32:**W606–W609.
7. **Cunningham, W. C., and J. W. Thanassi.** 1979. Synthesis of 5′-deoxypyridoxal derivatives. Experientia **35:**451–452.
8. **Di Salvo, M. L., S. Hunt, and V. Schirch.** 2004. Expression, purification and kinetic constants for human and *Escherichia coli* pyridoxal kinases. Prot. Express. Purif. **36:**300–306.
9. **Esnouf, R. M.** 1997. An extensively modified version of MolScript that includes greatly enhanced coloring capabilities. J. Mol. Graph. **15:**132–134.
10. **Laine-Cessac, P., and P. Allain.** 1996. Kinetic studies of the effects of K^+, Na^+ and Li^+ on the catalytic activity of human erythrocyte pyridoxal kinase. Enzyme Protein **49:**291–304.
11. **Li, M.-H., F. Kwok, W.-R. Chang, S.-Q. Liu, S. C. L. Lo, J.-P. Zhang, T. Jiang, and D.-C. Liang.** 2004. Conformational changes in the reaction of pyridoxal kinase. J. Biol. Chem. **279:**17459–17465.
12. **Li, M.-H., F. Kwok, W. R. Chang, C. K. Lau, J. P. Zhang, S. O. Liu, Y. C. Leung, T. Jiang, and D. C. Liang.** 2002. Crystal structure of brain pyridoxal kinase, a novel member of the ribokinase superfamily. J. Biol. Chem. **277:**46385–46390.
13. **Mathews, I. I., M. D. Erion, and S. E. Ealick.** 1998. Structure of human adenosine kinase at 1.5 Å resolution. Biochemistry **37:**15607–15620.
14. **McCormick, D. B., M. Gregory, and E. E. Snell.** 1961. Pyridoxal phosphoki-

nases. I. Assay, distribution, purification, and properties. J. Biol. Chem. **236:**2076–2084.
15. **McCormick, D. B., and E. E. Snell.** 1961. Pyridoxal phosphokinases. II. Effects of inhibitors. J. Biol. Chem. **236:**2085–2088.
16. **Merrit, E. A., and M. E. P. Murphy.** 1994. Raster3D version 2.0: a program for photorealistic molecular graphics. Acta Crystallogr. D **50:**869–873.
17. **Navaza, J.** 1994. AMoRe: an automated package for molecular replacement. Acta Crystallogr. D **50:**157–163.
18. **Notredame, C., D. Higgins, and J. Heringa.** 2000. T-Coffee: a novel method for fast and accurate multiple sequence alignment. J. Mol. Biol. **302:**205–217.
19. **Pearson, W. R.** 1990. Rapid and sensitive sequence comparison with FASTP and FASTA. Methods Enzymol. **183:**63–98.
20. **Safo, M. K., F. N. Musayev, S. Hunt, M. L. di Salvo, N. Scarsdale, and V. Schirch.** 2004. Crystal structure of the PdxY protein from *Escherichia coli*. J. Bacteriol. **186:**8074–8082.
21. **Sali, A., and T. L. Blundell.** 1993. Comparative protein modelling by satisfaction of spatial restraints. J. Mol. Biol. **234:**779–815.
22. **Schumacher, M. A., D. M. Scott, I. I. Mathews, S. E. Ealick, D. S. Roos, B. Ullman, and R. G. Brennan.** 2000. Crystal structures of *Toxoplasma gondii* adenosine kinase reveal a novel catalytic mechanism and prodrug binding. J. Mol. Biol. **298:**875–893.
23. **Sigrell, J. A., A. D. Cameron, T. A. Jones, and S. L. Mowbray.** 1998. Structure of *Escherichia coli* ribokinase in complex with ribose and dinucleotide determined to 1.8 Å resolution: insights into a new family of kinase structures. Structure **6:**183–193.
24. **Sivaraman, J., Y. Li, J. Banks, D. E. Cane, A. Matte, and M. Cygler.** 2003. Crystal structure of *Escherichia coli* PdxA, and an enzyme involved in the pyridoxal phosphate biosynthesis pathway. J. Biol. Chem. **278:**43682–43690.
25. **Yang, E. S., and V. Schirch.** 2000. Tight binding of pyridoxal 5′-phosphate to recombinant *Escherichia coli* pyridoxine 5′-phosphate oxidase. Arch. Biochem. Biophys. **377:**109–114.
26. **Yang, Y., H. C. Tsui, T. K. Man, and M. E. Winkler.** 1998. Identification and function of the *pdxY* gene, which encodes a novel pyridoxal kinase involved in the salvage pathway of pyridoxal 5′-phosphate biosynthesis in *Escherichia coli* K-12. J. Bacteriol. **180:**1814–1821.
27. **Yang, Y., G. Zhao, and M. E. Winkler.** 1996. Identification of the *pdxK* gene that encodes pyridoxine (vitamin B_6) kinase in *Escherichia coli* K-12. FEMS Microbiol. Lett. **141:**89–95.
28. **Zhang, Y., M. Dougherty, D. M. Downs, and S. E. Ealick.** 2004. Crystal structure of an aminoimidazole riboside kinase from *Salmonella enterica*: implications for the evolution of the ribokinase superfamily. Structure **12:** 1809–1821.